Gas-solid carbonation as a possible source of carbonates in cold planetary environments

Alexandre Garenne, German Montes-Hernandez, Pierre Beck, Bernard
Schmitt, Olivier Brissaud, Antoine Pommerol

HAL Id: insu-00761028

https://hal-insu.archives-ouvertes.fr/insu-00761028

Gas-solid carbonation as a possible source of carbonates in cold planetary environments

A. Garenne[a, *], G. Montes-Hernandez[a, *], P. Beck[b], B. Schmitt[b], O. Brissaud[b], A. Pommerol[c]

[a] CNRS and University Joseph Fourier, ISTerre/UMR 5275, OSUG/INSU, BP 53, 38041 Grenoble Cedex 9, France

[b] CNRS and University Joseph Fourier, IPAG, OSUG/INSU, BP 53, 38041 Grenoble Cedex 9, France

[c] Physikalisches Institut, Universität Bern, Sidlerstrasse 5, CH-3012 Bern, Switzerland

*Corresponding authors: A. Garenne and G. Montes-Hernandez

Tel: Alexandre.Garenne: +33 (0)607912561

German. Montes-Hernandez : +33 (0)683363044

E-mail addresses: alexandre.garenne@obs.ujf-grenoble.fr and german.montes-hernandez@obs.ujf-grenoble.fr

1

Abstract

Carbonates are abundant sedimentary minerals at the surface and sub-surface of the Earth and they have been proposed as tracers of liquid water in extraterrestrial environments. Their formation mechanism is since generally associated with aqueous alteration processes. Recently, carbonate minerals have been discovered on Mars' surface by different orbital or rover missions. In particular, the phoenix mission has measured from 1 to 5% of calcium carbonate (calcite type) within the soil (Smith P.H. et al., 2009). These occurrences have been reported in area were the relative humidity is significantly high (Boynton et al., 2009). The small concentration of carbonates suggests an alternative process on mineral grain surfaces (as suggested by Shaheen et al., 2010) than carbonation in aqueous conditions. Such an observation could rather point toward a possible formation mechanism by dust-gas reaction under current Martian conditions. To understand the mechanism of carbonate formation under conditions relevant to current Martian atmosphere and surface, we designed an experimental setup consisting of an infrared microscope coupled to a cryogenic reaction cell (IR-CryoCell setup). Three different mineral precursors of carbonates (Ca and Mg hydroxides, and a hydrated Ca silicate formed from Ca_2SiO_4), low temperature (from -10 to +30°C), and reduced CO_2 pressure (from 100 to 2000 mbar) were utilized to investigate the mechanism of gas-solid carbonation at mineral surfaces. These mineral materials are crucial precursors to form Ca and Mg carbonates in humid environments (0 < relative humidity < 100%) at dust-CO_2 or dust-water ice-CO_2 interfaces. Our results reveal a significant and fast carbonation process for Ca hydroxide and hydrated Ca silicate. Conversely, only a moderate carbonation is observed for the Mg hydroxide. These results suggest that gas-solid carbonation process or carbonate formation at the dust-water ice-CO_2 interfaces could be a

2

48   currently active Mars' surface process. To the best of our knowledge, we report for the first time

49   that calcium carbonate can be formed at a negative temperature (-10°C) via gas-solid carbonation

50   of Ca hydroxide. We note that the carbonation process at low temperature (<0°C) described in the

51   present study could also have important implications on the dust-water ice-CO2 interactions in

52   cold terrestrial environments (e.g. Antarctic).

53

54

55

56

57

58

61

62

63

64

65

1. Introduction

The biotic and abiotic (i.e. chemical) formation of carbonates plays a crucial role in the global carbon cycle on Earth. In addition, carbonate minerals often sequester various trace elements (actinides and lanthanides), metalloids, and heavy metals, and thus control in part their global cycling (e.g. Paquette and Reeder, 1995; Stumm and Morgan, 1995; Sigg et al., 2000). In general, carbonate minerals can be formed in natural or artificial environments by three different mechanisms (e.g. Montes-Hernandez et al., 2010a): (1) aqueous nucleation-growth in homogeneous or heterogeneous systems (aqueous conditions), for example, the chemical or biogenic formation of carbonates in lakes, oceans, CO_2 storage sites, natural caves; (2) gas-solid carbonation of alkaline minerals (fine particles) in the presence of adsorbed water (water humidity conditions, $0 <$ water activity < 1), for example carbonate formation in water-unsaturated soils, in terrestrial or extraterrestrial aerosols (Shaheen et al., 2010). This water has an important role in the surface chemistry of minerals as was shown by Galhotra et al., (2009) and Baltrusaitis and Grassian (2005) with zeolites and iron oxide surfaces; (3) dry gas-solid carbonation of granular/porous materials (dry conditions, water activity ≈ 0), for example, the industrial mineralization, recovery or capture of CO_2 at high temperatures in presence of alkaline binary oxides (CaO, MgO) or metastable, nanoparticle alkaline silicates (Montes-Hernandez et al., 2012).

In the Planetary Sciences context, carbonates are generally considered as indicators of aqueous alteration processes (Bandfield et al., 2003; Milliken and Rivkin, 2009; Boynton et al., 2009; Ehlmann et al., 2008; Michalski and Niles, 2010). In the case of Mars, huge deposits of surface carbonates remained undetected for a long period, and their suspected absence was used

4

88   to constrain the chemistry of a putative Martian ocean (Fairén et al., 2004). Evidences are now

89   growing for the presence of carbonates at the surface of the red planet, which include

90   observations of carbonate-rich outcrops (Ehlmann et al., 2008; Michalski and Niles, 2010) as

91   well as carbonates within the Martian dust (Bandfield et al., 2003; Boynton et al., 2009). The

92   aqueous alteration of mafic rocks in the presence of CO_2 is certainly an efficient mechanism for

93   carbonate synthesis, an alternative pathway of carbonate synthesis exists, which does not require

94   the presence of liquid water. This pathway involves reaction of a mineral substrate with CO_2 in

95   the presence of chemisorbed water (few angstroms to few nm thick layers), and was recently

96   tested and observed for terrestrial aerosols (Shaheen et al., 2010).

97   Here, we report on an experimental study of the kinetic of carbonation in liquid-water free

98   environment. We designed novel, state of the art experimental setup (IR-CryoCell) to investigate

99   the *in-situ* gas-solid carbonation (i.e. resolved in time), for temperature and pressure conditions

100   relevant to Mars. We studied carbonate synthesis starting from Ca and Mg hydroxides and an

101   amorphous silicate (synthesized from Ca_2SiO_4), at low temperature (from -10 to +30°C) and at

102   low CO_2 pressure (from 100 to 2000 mbar). These starting materials are known precursors to

103   form respective Ca and Mg carbonates in humid environments at dust-CO_2 or dust-water ice-CO_2

104   interfaces, at least under « terrestrial » conditions. They also can be expected to occur at the

105   surface of Mars and some asteroids (Mg hydroxide has been described on Ceres). We report here

106   laboratory experiments on gas-solid carbonation process at low temperature (<0°C), which

107   provides new insights on conditions for carbonate formation. We will show that gas-solid

108   carbonation can occur below the water frost point (at terrestrial atmospheric pressure), with

109   significant implications on the dust/water-ice/CO_2 interactions in cold environments.

5

2. Materials and methods

110   **2. Materials and methods**

111   The experiments were performed using three different materials, Ca, Mg hydroxide and a Ca

112   silicate hydrate. CO_2 is known to react with surface of CaO and MgO by adsorption (Ochs et al.,

113   1998a; Ochs et al., 1998b) and produce carbonates as well the importance of OH groups to water

114   adsorption on surfaces (Yamamoto et al., 2008). These substrates were chosen to mimic natural

115   conditions and to catalyze reaction as their surfaces are terminated by OH groups: i) in order to

116   form Ca-Mg carbonate by reaction with CO_2, a Ca and Mg source is needed; ii) the presence of

117   hydroxyl groups in the starting material was requested to permit auto-catalysis of the reaction

118   (Montes-Hernandez et al., 2010a); iii) the material had to be geologically relevant.

119   Brucite has not been detected on the Martian surface. However, various types of phyllosilicates

120   have been now described over the planet, that are interpreted as aqueous alteration products of

121   mafic rocks (see the recent review by Ehlmann et al., 2011). Such aqueous alteration processes

122   can be accompanied by the production of brucite (Evans, 2008). Identification of brucite by its

123   spectral properties is difficult since no diagnostic band is present in the NIR, with the exception

124   of the 2.7 micrometer feature ubiquitous to almost all -OH bearing phases. Brucite has been

125   diagnosed on some asteroids from observations in the mid-IR (together with carbonate). It is the

126   case of the largest main-belt object, Ceres. In addition, MgO has been proposed as a condensation

127   product in some solar nebula models, which should readily transform to brucite in the presence of

128   gaseous water or humidity (Gail and Sedlmayr, 1999).

129   Portlandite has not been reported on Mars either. On Earth, it is almost always found in

130   association with calcium carbonates, and is very difficult to observe due to its high reactivity with

131   CO_2. We chose to study portlandite because of its high catalytic reactivity which enabled to

132 provide kinetic measurements under some hours. In addition, it is a structural analog to brucite

133 and a number of X-$(OH)_2$ type hydroxide compounds (where X=Ni, Co, Fe, Mn, Cd). CaO has

134 also been proposed as an intermediate compound by Shaheen et al. (2010) to explain the

135 formation of calcium carbonate on Mars, which could readily transform to portlandite in the

136 presence of gaseous H_2O or humidity.

137 Finally, we used an amorphous calcium silicate hydrate synthesized from larnite (Ca_2SiO_4). This

138 material was chosen to represent an amorphous volcanic material. Volcanic activity has been

139 widespread on Mars, and volcanoclastic deposits have been described (Ehlmann et al., 2011). We

140 decided to use a pure calcium amorphous silicate (rather than a basaltic glass), in order to

141 simplify the chemistry of the system. However, one might expect a more complex chemistry for

142 Martian volcanic glasses. Our approach might appear too simplistic, but might provide grounds

143 for understanding more complex chemistries.

144

145 2.1. Materials

146 **Portlandite:** Calcium hydroxide $Ca(OH)_2$ was provided by Sigma-Aldrich with 96% chemical

147 purity (about 3% of $CaCO_3$) and 1% of other impurities. This material is characterized by platy

148 nanoparticles (sheet forms) forming micrometric aggregates with high porosity and/or high

149 specific surface area (15 m^2/g). Its infrared spectrum has revealed a small amount of adsorbed

150 water at atmospheric conditions, around $0,01gH_2O/gCa(OH)_2$ determinated by TGA. The

151 portlandite sample was used without any physicochemical treatment.

152 **Brucite:** Magnesium hydroxide $Mg(OH)_2$ was provided by Fisher Scientific (UK). This material

7

153 is characterized by platy hexagonal microparticles. A small amount of adsorbed water at

154 atmospheric conditions was detected by infrared spectroscopy. The brucite sample was crushed in

155 a mortar before use.

156 **Amorphous calcium silicate hydrate:** This material was synthesized from synthetic larnite

157 mineral (Ca_2SiO_4) by using a simple acidic treatment (2M HCl solution) at room lab temperature

158 during 15 minutes. Then, consecutive dilutions with demineralized water were carried out until

159 pH equal to 3. Finally, the solid was separated from the solution by centrifugation (10 minutes at

160 12000 rpm) and dried directly in the centrifugation flasks at 80°C for 48h. The larnite synthetic

161 mineral was provided by A. Santos and it was synthesized as reported in Santos et al. (2009).

162 **Carbon dioxide:** Carbon dioxide CO_2 was provided by Linde Gas S.A. with 99.995% of

163 chemical purity. This gas was directly injected in the cryogenic reaction cell without any

164 treatment or purification.

165 *2.2. Infrared microscope*

166 An infrared microscope (BRUKER HYPERION 3000) coupled with a cryogenic cell (designed

167 and built at IPAG) was used to obtain infrared spectra in transmission mode. The IR beam was

168 focused trough a 15x objective and the typical size of the spot on the sample was around 50x50

169 μm^2. The spectral resolution was $4cm^{-1}$ and the spectra were recorded in transmission mode

170 between $4000cm^{-1}$ and $700cm^{-1}$.

171 *2.3. Cryogenic cell*

172 An environmental cell was designed and built at IPAG in order to simulate low CO_2 pressure and

173   low temperature (LP-LT) close to Martian atmospheric conditions. A heating resistance coupled

174   to a liquid N_2 circuit (77K) allows an efficient regulation of sample temperature from -180°C to

175   +100°C. Additionally, a turbomolecular vacuum pump and a CO_2 cylinder were connected to

176   reach a secondary vacuum and to inject a controlled CO_2 pressure into the reaction cell,

177   respectively. Figure 1 shows a schematic diagram of all main parts of the IR-CryoCell setup.

178   *2.4. Gas-solid carbonation experiments*

179   For these measurements, the reacting $Ca(OH)_2$ particles, stored at atmospheric conditions, were

180   manually deposited and compressed as a thin film on a KBr window. Then the KBr window was

181   carefully placed in the reaction cell to be assembled to the microscope. All carbonation

182   experiments have been carried out in presence of molecular water (adsorbed or crystallized as ice

183   depending on the carbonation temperature) which catalyze the carbonation process. The

184   carbonation temperatures used in this study were -10, 0, 10, 25 or 30°C and the CO_2 pressures

185   were typically 100, 1000 and 2000 mbar. This pressure is higher than Martian pressure to

186   accelerate the reaction due to a daily timescale limitation by the experimental setup. We note that

187   the CO_2 gas has been directly injected into the reaction cell in presence or absence of atmospheric

188   air. For the latter case, we started by fixing the water adsorbed onto the solid by cooling the cell

189   at -60°C before making a high vacuum pumping for 10 min in order to remove exclusively the air

190   from the reaction cell. After injection of CO_2 10 to 15 infrared spectra have been collected as a

191   function of time until an apparent spectroscopic equilibrium state is reached (3-6h).

192   Complementary carbonation experiments have been carried out by using Mg hydroxide (brucite:

193    $Mg(OH)_2$) and the amorphous calcium silicate hydrate as solid reactants, but, for these cases the

194   carbonation temperature has been fixed at 25°C and 1 bar of CO_2 has been injected into the

9

195 reaction cell without air removal (more reacting system).

196 Each carbonation experiment has been repeated 2 times in order to verify its reproducibility. All

197 carbonation experiments and their physicochemical conditions are summarized in Table 1.

198 *2.5. Calculation of integrated band intensities*

199 The gas-solid carbonation of calcium hydroxide at low temperature (<30°C) in presence of

200 adsorbed water can be expressed by a global reaction as follows:

201 $Ca(OH)_2(s) + CO_2(g) => CaCO_3 (s) + H_2O (v-l)$ (1)
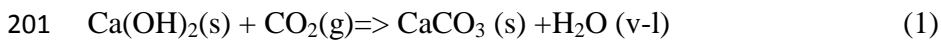
202 Generally, this global reaction is incomplete due to the formation of a protective carbonate layer

203 around the reacting particle which restricts or stops the CO_2 transfer at the grain or aggregate

204 scale (Montes-Hernandez et al., 2010a). In the present study, the integrated band intensities for

205 hydroxyl (-OH), carbonate (CO_3^{2-}) and H_2O functional groups, concerning reaction (1) at an

206 instant *t* have been estimated by using a Trapezoidal rule integration. A wavenumber interval and

207 a characteristic continuum have been manually defined to determine the intensity of a given band

208 depending on the initial reactant. For example, in the gas-solid carbonation experiments with

209 $Ca(OH)_2$ particles, two continuums have been defined as linear segments over two different

210 spectral ranges, one for the -OH at 3640 cm^{-1} and H_2O at 3450 cm^{-1} band intensities and the other

211 for the H_2O at 1650 cm^{-1} and CO_3^{2-} at 1420 cm^{-1} band intensities (see Figure 2).

212

213 *2.6. Fitting of the kinetic experimental-calculated data for gas-solid carbonation*

214 Several kinetic models (first-order, pseudo-first-oder, second-order, pseudo-second-order,

215 reversible one, irreversible one...) are generally used for fitting kinetic experimental data of

216 sorption and adsorption systems (Ho and McKay, 1999; Ho, 2006). For our experiments, we

10

217   have chosen pseudo-second-order model because it was successfully applied in previous studies

218   (Montes-Hernandez and Geraud, 2004 ; Montes-Hernandez and Rihs, 2006; Montes-Hernandez

219   et al., 2009, 2010a, 2010b, 2012a, 2012b) and can be adequately used to fit experimental data of

220   carbonation process as demonstrated in Montes-Hernandez et al., 2009. This model reproduces a

221   process consisting of a fast mass transfer followed by a second step of slower mass transfer until

222   equilibrium is achieved. It can be written in its differential form as follows:

$$\frac{dA^{CO3}{}_{,t}}{dt} = Kc \left(A^{CO3}{}_{,max} - A^{CO3}{}_{,t} \right)^2$$

223   (2)

224   Where $A^{CO3}{}_{,t}$ is the integrated band intensity for the carbonate group at a given time, t [minutes],

225   corresponding to carbonation extent; $A^{CO3}{}_{,max}$ is the maximum extend of carbonation at

226   equilibrium; Kc is the rate constant of $Ca(OH)_2$ carbonation.

227   The second step (until equilibrium) is interpreted by as a passivation effect due to the formation

228   of a protective carbonate layer (Montes-Hernandez et al., 2012a). In this study, the increase of

229   integrated band intensity with time for the carbonate group (CO_3^{2-}), i.e. during gas-solid

230   carbonation process, has been fitted by using a kinetic double-pseudo-second-order model. This

231   model assumes two kinetic regimes due to the presence of two types of reactive surface sites. The

232   integrated form of the double kinetic model is given by the following hyperbolic equation:

$$A^{CO3}{}_{,t} = \frac{\left(A^{CO3}{}_{,max1} \right)t}{\left(t_{1/2_1} + t \right)} + \frac{\left(A^{CO3}{}_{,max2} \right)t}{\left(t_{1/2_2} + t \right)}$$

233   (3)

234   Where $A^{CO3}{}_{,t}$ is the integrated band intensity for the carbonate group at a given time, t [minutes],

11

235 corresponding to carbonation extent; $A^{CO3}_{,max1}$ and $A^{CO3}_{,max2}$ are the maximum extent of

236 carbonation at apparent equilibrium for both kinetic carbonation regimes, respectively; $t_{1/2_1}$ and

237 $t_{1/2_2}$ are the half-carbonation times for both kinetic carbonation regimes, respectively. In other

238 terms, the half-carbonation times represent the times after which half of the maximum of kinetic

239 carbonation regimes (expressed as maximum of integrated band intensities for carbonate group)

240 is obtained. The fitting of kinetics data allow an estimation of these parameters and was

241 performed by a non linear regression by least-squares method. These simple parameters are used

242 in this study to evaluate the kinetic effects of temperature, CO_2 pressure and nature of the solid

243 on the gas-solid carbonation process.

244 The activation energy (Ea, Table 1) of the reaction was calculated assuming an Arrhenius

245 behavior for the initial carbonation rate. We have used 4 points to calculate Ea for carbonation

246 experiments of portlandite (at the temperature of -10°C,0°C,10°C and 30°C, for both experiments

247 performed under 1 bar and 2 bar CO_2).

248

249 **3. Results**

250

251 *3.1. Gas-solid carbonation of Ca(OH)₂ particles at low temperature (<0°C)*

252 Very few experimental studies have characterized the carbonate formation or CO_2 mineralization

253 at the mineral-ice water-CO_2 interfaces on Earth and planetary cold-environments (e.g. Antarctic

254 and Mars surface). In our study, several gas-solid reactions carried out in the cryogenic cell

255 coupled to the infrared microscope reveal that carbonate formation or CO_2 mineralization is

256 possible at low temperature (-10°C and 0°C) using a simplified analogue Ca(OH)₂(mineral)-

12

257 water(adsorbed)-CO_2(gas) system (see Fig. 3 (c) to (f)). The results displayed in Figure 3 also

258 reveal that the carbonation extent, monitored *in-situ* by an increase of carbonate band intensity at

259 1420 cm^{-1}, is clearly inhibited by a decrease of temperature from 30°C to -10 °C. The increase of

260 integrated band intensity with time for the carbonate group at 1420 cm^{-1} has been successfully

261 fitted by using the kinetic double-pseudo-second-order model. The experimental data and the

262 calculated fits for six experiments are plotted in Figure 4. This "a posteriori" modeling shows the

263 good fits of all the experimental data by such type of kinetic model (correlation coefficient, R

264 close to 1), and confirms the inhibition effect of temperature and the effect of relative humidity

265 on the carbonation extent and kinetic parameters (see also Table 1).

266 One additional carbonation experiment with $Ca(OH)_2$ particles was carried out at low CO_2

267 pressure (100 mbar) and at moderate temperature (25°C). For this case, the initial air contained

268 into the cell was previously removed by pumping to secondary vacuum at low temperature (-

269 60°C) as explained in the materials and methods section. Here, a significant carbonation is

270 observed after 4 minutes of $Ca(OH)_2$-CO_2 interaction followed by a very slow carbonation step

271 until an apparent spectroscopic equilibrium is possibly reached (about 6h) (see Fig. 5). These

272 experimental data have been also successfully fitted by using the kinetic double-pseudo-second-

273 order model. A last carbonation experiment was performed at a CO_2 pressure of 2 bar (at 25 °C)

274 in order to compare with the low CO_2 pressure experiments. A significant carbonation was

275 observed during all the experiment (see Fig. 6), which was fitted with the kinetic-pseudo-second

276 order model.

277 *3.2. Gas-solid carbonation of Mg hydroxide*

278 The gas-solid carbonation depends also on the nature of the solid. For this reason one other

13

279 powdered material, Mg hydroxide (synthetic brucite), was investigated specifically at higher

280 reactive conditions (25°C and 1bar of CO_2, in presence of air). To form Mg carbonates, the most

281 simple materials as starting reactant are binary oxides or hydroxides in the precursor material.

282 Brucite particles are found to be only slightly carbonated at these T-P_{CO2} conditions after 5.5h of

283 $Mg(OH)_2$-CO_2 interaction (see Figure 7). These *in-situ* infrared measurements clearly reveal that

284 the Mg hydroxide (brucite) is more chemically stable than Ca hydroxide (portlandite) under a

285 CO_2-rich atmosphere at a given relative humidity. In summary, the gas-solid carbonation of Ca

286 and Mg hydroxides depends on the experimental conditions employed (i.e. T, P_{CO2}, relative

287 humidity) and on the intrinsic properties of solid (i.e. hydrophilicity, particle size, specific surface

288 area, and chemical stability).

289 Finally, a kinetic regime and the maximum carbonation extent at an apparent equilibrium

290 ($A^{CO3}_{,max1}$ + $A^{CO3}_{,max2}$) is successfully determined by using a kinetic double-pseudo-second-order

291 model (see Fig. 7 (c)).

292 *3.3. Gas-solid carbonation of an amorphous calcium silicate hydrate*

293 A last materials, an amorphous calcium silicate hydrate, has been investigated at higher reactive

294 conditions (25°C and 1bar of CO_2, in presence of air) to test the gas-solid carbonation efficiency.

295 The amorphous calcium silicate hydrate, is significantly carbonated via gas-solid carbonation at

296 the above mentioned T-P_{CO2} conditions after 8h of reaction (see Figure 8), which suggests

297 chemical stability has a significant impact on the efficiency of the carbonation.

298 Finally, a kinetic regime and the maximum carbonation extent at apparent equilibrium ($A^{CO3}_{,max1}$

299 + $A^{CO3}_{,max2}$) is also successfully determined by using the kinetic double-pseudo-second-order

300 model (see Fig. 8 (c)).

301

14

4. The mechanism of carbonation

All the experiments with the Ca and Mg hydroxides show an increase of the band intensities of carbonates, at low temperature and low pressure. In this study we assume that part of the water initially adsorbed onto $Ca(OH)_2$ particles was partially crystallized by cooling when the temperature is negative ($<0°C$). The presence of an ice layer limits the access of CO_2 molecules to nanopores, and therefore limiting the CO_2 access to the local CO_3^{2-} production ($CO_2(g)+H_2O(adsorbed)=>CO_3^{2-}+2H^+$) required to form a carbonate layer around the $Ca(OH)_2$ particles (see also: Montes-Hernandez et al. 2010a). Strictly speaking, the relative humidity is not controlled in our experiments; however, two experiment protocols implying atmospheric vapor have been designed, firstly, direct injection of CO_2 gas into the reaction cell initially filled with air, i.e. at lab relative humidity (CO_2-air system) and secondly, the injection of CO_2 gas after removal of the air by secondary vacuum pumping at low temperature (-60°C) (CO_2 system). The difference between these experiments could explain why the carbonation extent decreases when the initial air (contained into the reaction cell) is removed (see comparisons (c) and (d) or (e) and (f) in Fig. 3). We can assume a similar relative humidity of the lab room for all experiments. The relative humidity has clearly an impact on the carbonation efficiency, the experiments without air (very low relative humidity) showing a lower amount of carbonation at low temperature.

The fit of the data by the kinetic model assumes two kinetic regimes, usually due to the presence of two types of reactive surface sites. In our carbonation experiments, the formation of a hydrated carbonate layer around the core of reacting $Ca(OH)_2$ particles produces a complex passivation step, possibly perturbed by three simultaneous physicochemical processes: (1) solid state transformation from hydrated calcium carbonate to calcite and/or from aragonite to calcite, (2) partial expelling of produced molecular water during the carbonation process (see Eq. (1)) and (3)

15

325   local acidification by an excess of molecular water in pores or onto surfaces (H_2O(produced)+

326   CO_2(g) =>HCO_3^- + H^+). In summary, the complex kinetic behavior related to gas-solid

327   carbonation of $Ca(OH)_2$ particles is successfully described applying two kinetic regimes. A

328   schematic representation of this carbonation process is illustrated in Figure 9. The rate of

329   carbonation depends on the access to the nanopores of the material by the CO_2. These pores have

330   to be water-unsaturated to facilitate access of the CO_2 gas to react with the minerals. The pressure

331   has a strong impact on the rate and yield of carbonation. In the case of the low pressure

332   experiments, a two stage kinetic model was shown to fit the data. Experiments revealed a fast

333   carbonation during a short time (stage 1) followed by a slower carbonation (stage 2). The

334   magnitude of carbonate formation is high in stage 1 and lower in stage 2. In the case of the

335   experiments performed at higher CO_2 pressure (2 bar) (fig. 6.c) a two stage reaction is also

336   observed. However, unlike the low pressure experiments, the magnitude of carbonation achieved

337   in stage 2 is quite significant.

338   For the low pressure experiments, we suspect that the intraparticle diffusion of CO_2, possibly

339   limited by the low gas pressure in the system (100 mbar of CO_2), is the rate limiting step due to

340   the carbonate layer which strongly reduce the diffusion of the gas. This rate limiting step is no

341   more observed at high CO_2 pressure (>20 bar). In this case, the $Ca(OH)_2$ particles are completely

342   carbonated, leading to the formation of calcite nano-crystals (Montes-Hernandez et al., 2010b).

343   We can assume a correlation between the pressure and the thickness of the layer that transforms

344   to carbonate by gas-solid reaction. The effect of CO2 pressure observed in explained by the

345   presence of passivation step and the formation of carbonate layer through which CO2 molecules

346   have to diffuse. Therefore in the case of an uncarbonated material, the effect of CO_2 pressure on

347   the initial reaction rate is expected to be moderate. Although the CO_2 pressure on Mars (about 10

16

348 mbar) is lower than CO_2 pressures used in our experiments (100 mbar), it is likely that our results

349 can be extrapolated to Martian atmospheric CO_2 pressure.

350

351 Unfortunately, the gas-solid carbonation mechanism of amorphous calcium silicate hydrate is not

352 elucidated due to its unknown atomic organization. However, we assume that the abundant

353 molecular water adsorbed onto the solid plays a crucial role to start the gas-solid carbonation

354 process at the investigated conditions. The *in-situ* infrared measurements reveal two important

355 insights: (1) The expelling of pre-existent molecular water in/on the solid towards the gas phase

356 during the carbonation process. This is attested by a clear decrease of the stretching and bending

357 band intensities of water (see Fig. 8 (a) and (b)), (2) Similar to carbonation of Ca hydroxide, the

358 formation of calcite and aragonite are mainly identified, the formation of hydrated calcium

359 carbonate being only suspected (see also Montes-Hernandez et al. 2010a)

360

361

362 *5. Discussion*

363

364   Carbonates have been found on Mars in two kinds of geological settings: (i) outcrops of

365 carbonates, identified in the Nili Fossae region (Ehlmann et al., 2008), in the central peak of

366 Leighton crater (Michalski and Niles, 2010) and in the Columbia Hills of Gusev crater (Morris et

367 al., 2010); and (ii) carbonates-bearing dust, identified by the TES instrument (Bandfield et al.,

368 2003) and the phoenix lander (Boynton et al., 2009). In the case of the outcrops from the

369 Columbia Hills and Nili Fossae, carbonates are present as major components (16 to 34 wt % in

370 the case of the Columbia Hills, about 80 % in the case of Nili Fossae), and their derived

17

371 chemistry is similar to that of carbonates found in Martian meteorites (Mittlefehldt, 1994), i.e.

372 Fe-Mg carbonates. The association of these carbonate outcrops with phyllosilicates advocate for a

373 possible hydrothermal origin of these carbonates, a phenomenon that has been reproduced in

374 laboratory experiments (Golden et al., 2000) and that is observed in some terrestrial hydrothermal

375 systems (Treiman et al., 2002; Brown et al., 2010). However, it is well known that terrestrial

376 alteration of mafic rocks can produce brucite as a primary alteration product (Xiong and Snider

377 Lord, 2008), which should readily transform into carbonate by interaction with the Martian

378 atmosphere, according to our experiments. The observed carbonates outcrops could rather be

379 former outcrops of brucite-rich sedimentary rocks, that were subsequently altered to carbonates

380 by interaction with the atmosphere.

381 In the case of carbonates observed in the Martian dust, both magnesite (Bandfield et al., 2003)

382 and calcite (Boynton et al., 2009) have been reported, and their typical abundance is below 5 %.

383 Although aqueous formation has received widespread attention for this type of occurrence of

384 carbonates on Mars, we propose gas-solid reaction as a possible formation mechanism. Calcite

385 formation at the dust-CO_2 interfaces requires a source of calcium (e.g. Ca binary oxides or an

386 amorphous metastable Ca silicate) possibly coming from volcanic activity (Shaheen et al., 2010),

387 mechanical erosion or extra-Martian particulate matter (including meteorite impacts, interstellar

388 dusts). A large diversity of phyllosilicates and hydrated phyllosilicates was found on the Martian

389 surface (Mustard et al., 2008; Jänchen et al., 2006; Fairén et al., 2009; Murchie et al., 2009;

390 Ehlmann et al., 2011). As we have shown, the presence of molecular water is also required

391 because hydration of the Ca precursor is assumed to be a crucial step prior to the carbonation

392 process. Laboratory studies of Martian analogs suggest that adsorbed water should be present in

393 significant amount within the Martian soil (Pommerol et al., 2009; Beck et al., 2010; Jänchen et

18

al., 2006) and adsorbed water has been also detected by infrared spectroscopy (Poulet et al., 2009). In addition, the gamma rays and neutrons spectrometers on Mars Odyssey have shown evidence for the presence of water in the first meter of the martian subsurface (Feldman et al., 2004). A simplified scenario for calcite formation at the dust-CO_2 interfaces and its natural deposition on the soil is schematically illustrated in Fig. 10. In this scenario we assume that the precursor, a calcium hydroxide with adsorbed water, is produced by atmospheric alteration of volcanic CaO particles in the atmosphere. Reactant minerals such as portlandite could be difficult to detect on Mars by reflectance spectroscopy due to the carbonate layer around the calcium hydroxide. In the case of hydromagnesite, the presence of brucite is required somewhere on Mars, which would be subsequently transformed to carbonates, eroded, and transported. As we stated earlier, brucite should form in association with phyllosilicates during the aqueous alteration of mafic rocks.

The efficiency of carbonates synthesis on Mars by gas-solid reaction will depend on the mineral substrate (as we showed, brucite, portlandite and larnite have distinct synthesis kinetics), the local temperature, the atmospheric humidity, and likely the atmospheric pressure (which can substantially vary with season as well as with topography). Even at temperatures below the frost point, carbonates synthesis can occur by gas-solid reaction, on a daily timescale (table 1). On Mars, the water vapor pressure is low (P_{H2O} about 10 Pa) and the frost point is depressed with regard to that on Earth. Given the present knowledge of the water vapor surface pressure, a typical value of 200 K is found for the frost point on the Martian surface (Schorghofer and Aharonson., 2005). Such temperature typically corresponds to seasonal average around 60° in latitude.

The relative humidity on Mars fluctuates on a daily basis. At the Phoenix landing site (Smith P.H.

19

417   et al., 2009) it is measured around 5% during Martian day time, close to saturation early night

418   and saturating at the end of the night. Carbonate synthesis will be accelerated by a high

419   atmospheric humidity, which can occur during the warmer season. TES instrument on Mars

420   Global Surveyor has water vapor evolution during 2 martian years, and the maximum was found

421   during midsummer in the northern hemisphere with 100 pr-µm (Smith M.D., 2002,2004). The

422   maximum water vapor measured by Mars Express instruments (OMEGA and SPICAM) is found

423   during midsummer, around 60 pr-µm content. This maximum is observed at latitude 75-80°N

424   and longitudes 210-240°E (Fouchet et al., 2007; Fedorova et al., 2006; Melchiorri et al.,2007)),

425   an area is close to Phoenix landing site (latitude 68°N and longitude 233°E).

426   Current Global Circulation Models (GCM) of Mars can be used to determine the optimal

427   locations and times for the gas-solid synthesis of carbonates. Simulations with Mars Climate

428   Database (Forget et al., 1999, 2006) estimated high relative humidity (around 70%) and

429   temperatures close to -20°C during mid summer (L_s =120°) in the Phoenix landing site area (at 12

430   a.m). These conditions are sufficient to initiate the carbonation reaction according to our

431   experiments, and carbonates were observed in the Phoenix soil (Smith et al., 2009)

432

433   Mars is not the only extra-terrestrial body where carbonates have been detected, this is

434   also the case of Ceres, the largest asteroid in the main belt. Its shape is close to hydrostatic

435   equilibrium and its bulk density suggests the presence of ice in its interior (Thomas et al., 2005).

436   The surface of Ceres shows a well-resolved 3-µm absorption band, which interpretation has been

437   debated (Lebofsky et al., 1981; Vernazza et al., 2005; Rivkin et al., 2006; Rivkin et al., 2011;

438   Beck et al., 2011). In a recent study, Milliken and Rivkin (2009) combined NIR and MIR

439   observations of Ceres' surface and successfully modeled both spectral regions with a combination

440 of brucite, carbonate and a Fe-rich phyllosilicate. Such a mineralogical assemblage was explained

441 by aqueous alteration of mafic silicates in the presence of CO_2, by analogy with the processes

442 inferred from the mineralogy of hydrated meteorites that can present a significant amount of

443 carbonates (Zolensky et al., 2002). If brucite is rare in the mineralogy of hydrated chondrites, it is

444 a common product of aqueous alteration of terrestrial rocks. The condition of brucite formation is

445 specific in terms of T, pH and pO_2, and source rock. If the formation of carbonate by reaction of

446 brucite with water is possible, gas-solid reaction cannot be excluded. This mechanism could

447 occur at some depth in the asteroid body, where CO_2 pressure can build-up. However, because of

448 the low temperature at the surface of Ceres, long timescales are expected for such a process.

449 Further consideration would require an accurate knowledge of the kinetics of the gas-solid

450 carbonation.

451

452 Finally, the carbonate synthesis mechanism that we described is certainly active on Earth,

453 where carbonate minerals played an important role in the planet evolution. Many studies are

454 available about carbonate reactivity and synthesis in liquid-water but information on its behavior

455 at sub-zero temperatures (for example solubility in frozen water) are sparse. The results we

456 obtained reveal that gas-solid carbonation can occur at sub-zero temperature, in the presence of

457 gaseous CO_2 and H_2O. These conditions are present on Earth in arctic regions and in the upper

458 atmosphere. This mechanism can thus occur on the availability of the adequate precursor.

459 The presence of oxygen isotope anomalies in carbonates from terrestrial aerosols

460 (Shaheen et al., 2010) suggests a carbonation by exchange with ozone. Such a result suggests a

461 possible formation of carbonate by chemical reaction in the upper atmosphere, from a CaO

462 precursor. We can propose hydration of $CaO_{(s)}$ by $H_2O_{(g)}$, and successive reaction of $Ca(OH)_{2(s)}$

21

463 with $CO_{2(g)}$ as a formation mechanism of these carbonates.

464   Calcium carbonate and carbonate hydrates have been found in arctic ice (Dieckmann et

465 al., 2008; Sala et al. 2008). The formation mechanism of these carbonates is a matter of active

466 research, since it could provide a major CO_2 sequestration process. Hydrous carbonates (for

467 instance ikaite) have been proposed to originate by precipitation during sea-ice formation, as

468 suggested by thermodynamical calculations. Anhydrous carbonates can have an origin as primary

469 aerosols, with a synthesis mechanism possibly similar to the one described in the previous

470 paragraph. In addition, in situ gas-solid formation is possible, depending on the availability of an

471 adequate precursor (as we showed here, an Ca or Mg hydroxides, or Ca-rich amorphous

472 silicates).

473

474 **6. Conclusion**

475 In this study, we designed an original experimental method to form carbonates via gas-solid

476 reaction in presence of adsorbed water. We used an infrared microscope coupled to a cryogenic

477 reaction cell (IR-CryoCell setup) to investigate this process with 3 different carbonate precursors

478 (Ca hydroxide (portlandite), Mg hydroxide (brucite), and an amorphous calcium silicate hydrate).

479 We demonstrated for the first time that calcium carbonate can be formed at low temperature

480 (<0°C) via gas solid carbonation of Ca hydroxide. Both amorphous Ca silicate hydrate and Ca

481 hydroxide were significantly carbonated at the investigated T-P_{CO2} conditions. Conversely, only a

482 very slight gas-solid carbonation of Mg hydroxide particles was detected by IR spectroscopy. We

483 extracted the kinetic parameters of the reaction from our measured carbonation curves, following

484 a kinetic double-pseudo-second-order model. From these results we can clearly state that the

485 conditions for gas-solid carbonation exist on Mars, and that this process could be the source of

486 the detected Ca and Mg carbonates found in the Martian dust and soil. These carbonates can be

487 synthesized from a brucite precursor (a common hydrothermal product), from volcanic derived

488 aerosols, as well as from extraterrestrial dust. This mechanism should be considered in future

489 global modeling of the carbon cycle of the red planet, and might also be active in cold terrestrial

490 deserts.

491

492 **Acknowledgements**

496

497 **References**

498 Bandfield, J.L., Glotch, T.D. and Christensen, P.R. , 2003. Spectroscopic Identification of

499   Carbonate Minerals in the Martian Dust. Science. 301, 1084-1087.

500 Beck, P., Pommerol, A., Schmitt, B. and Brissaud, O., 2010. Kinetics of water adsorption on

501   minerals and the breathing of the Martian regolith. J.Geophys. Res.-Planets. 115, E10011

502 Beck, P., Quirico, E., Sevestre, D., Montes-Hernandez, G., Pommerol, A. and Schmitt, B. 2011.

503   Goethite as an alternative origin of the 3.1mu m band on dark asteroids. Astron.

504   Astrophys. 526, A85.

505 Baltrusaitis, J. and Grassian, V.H., 2005. Surface reactions of carbon dioxide at the adsorbed

506   water-iron oxide interface. J Phys Chem B. 109, 12227–12230.

507   Boynton, W. V., Ming, D. W., Kounaves, S. P., Young, S. M. M., Arvidson, R. E., Hecht, M. H.,

508   Hoffman, J., Niles, P. B., Hamara, D. K., Quinn, R. C., Smith, P. H., Sutter, B., Catling, D. C.

509   and Morris, R. V., 2009 Evidence for Calcium Carbonate at the Mars Phoenix Landing

510   Site. Science. 325, 61-64.

511   Brown, A. J., Hook, S. J., Baldridge, A. M., Crowley, J. K., Bridges, N. T., Thomson, B. J.,

512   Marion, G. M., de Souza Filho, C. R. and Bishop, J. L., 2010. Hydrothermal formation of

513   Clay-Carbonate alteration assemblages in the Nil Fossae region of Mars. Earth Planet.

514   Sci. Lett. 297, 174-182.

515   Dieckmann, G.S., Nehrke, G., Papadimitriou, S., Göttlicher, J., Steininger, R., Kennedy, H.,

516   Wolf-Gladrow, D. and Thomas, D.N., 2008. Calcium carbonate as ikaite in Antartic sea

517   ice. Geophys. Res. Lett.35, L08501.

518   Ehlmann, B.L., Mustard, J.F., Murchie, S.L., Poulet, F., Bishop, J.L., Brown, A.J., Calvin, W.M.,

519   Clark, R.N., Des Marais, D.J., Milliken, R.E., Roach, L.H., Roush, T.L., Swayze, G.A.

520   and Wray, J.J., 2008. Orbital Identification of Carbonate-Bearing Rocks on Mars.

521   Science. 322, 1828-1832.

522   Ehlmann, B.L., Mustard, J.F., Murchie, S.L., Bibring, J.-P., Meunier, A., Fraeman, A.A. and

523   Langevin, Y., 2011. Subsurface water clay mineral formation during the early history of

524   Mars. Nature. 479, 53-60.

525   Evans, B.W., 2008. Control of the products of serpentinization by the Fe(2)Mg(1) exchange

526   potential of olivine and orthopyroxene. J. Petrol. 49, 1873-1887.

527   Fairén, A. G., Fernandez-Remolar, D., Dohm, J. M., Baker, V. R. and Amils, R., 2004. Inhibition

24

528   of carbonate synthesis in acidic oceans on early Mars. Nature. 431, 423-426.

529   Fairén, A.G., Davila, A.F., Gago-Duport, L., Amils, R. and McKay, C.P., 2009. Stability against

530   freezing of aqueous solutions on early Mars. Nature.459,401-404.

531   Fedorova, A., Korablev, O., Bertaux, J.-L., Rodin, A., Kiselev, A. and Perrier, S., 2006. Mars

532   water vapor abundance from SPICAM IR spectrometer: Seasonnal and geographic

533   distributions. J. Geophys. Res.111, E09S08.

534   Feldman, W.C., Prettyman, T.H., Maurice, S., Plaut, J.J., Bish, D.L., Vaniman, D.T., Mellon,

535   M.T., Metzger, A.E., Squyres, S.W., Karunatillake, S., Boynton, W.V., Elphic, R.C.,

536   Funsten, H.O. Lawrence, D.J. and Tokar, R.L., 2004. Global distribution of near-surface

537   hydrogen on Mars. J. Geophys. Res.109, E09006.

538   Forget, F., Hourdin, F., Fournier, R., Hourdin, C., Talagrand, O., Collins, M., Lewis, S. R., Read,

539   P. L., & Huot, J.-P. 1999. Improved general circulation models of the Martian atmosphere

540   from the surface to above 80 km. Journal of Geophysical Research, 1042, 24155–24176.

541   Forget, F., Millour, E., Lebonnois, S., Montabone, L., Dassas, K., Lewis, S. R., Read, P. L.,

542   López-Valverde, M. A., González-Galindo, F., Montmessin, F., Lefèvre, F., Desjean, M.-

543   C., & Huot, J.-P. 2006 (Feb.). The new Mars climate database. Page 128 of : F. Forget, M.

544   A. Lopez-Valverde, M. C. Desjean, J. P. Huot, F. Lefevre, S. Lebonnois, S. R. Lewis, E.

545   Millour, P. L. Read, & R. J. Wilson (ed), Mars Atmosphere Model ling and Observations.

546   Fouchet, T., Lellouch, E., Ignatiev, N.I., Forget, F., Titov, D.V., Tschimmel, M., Montmessin, F.,

547   Formisano, V., Guiranna, M., Maturilli, A. and Encrenaz, T., 2007. Martiann water vapor:

548   Mars Express PFS/LW observations. Icarus. 190, 32-49.

549   Gail, H.-P. and Sedlmayr, E., 1999. Mineral formation in stellar winds. Astron. Astrophys. 347,

550   594–616.

25

551 Galhotra, P., Navea, J.G., Larsen, S.C. And Grassian,V.H. , 2009. Carbon dioxide ((CO2)-O-16

552 and (CO2)-O-18) adsorption in zeolite Y materials: Effect of cation, adsorbed water and

553 particle size. Energ Environ Sci .2,401–409.

554 Golden, D. C., Ming, D. W., Schwandt, C. S., Morris, R. V., Yang, S. V. and Lofgren, G. E.,

555 2000. An experimental study on kinetically-driven precipitation of calcium-magnesium-

556 iron carbonates from solution: Implications for the low-temperature formation of

557 carbonates in martian meteorite Allan Hills 84001. Meteoritics Planet. Sci. 35, 457-465.

558 Ho, Y.S. and McKay, G., 1999. Pseudo-second order model for sorption processes. Process

559 Biochem. 34, 451-465

560 Ho, Y.S., 2006. Review of second order models for adsorption systems. J. Hazard Mater. B136,

561 681-689

562 Jänchen, J., Bish, D.L., Möhlmann, D.T.F. and Stach, H., 2006. Investigation of the water

563 sorption properties of Mars-relevant micro-and mesoporous minerals. Icarus. 180, 353-

564 358.

565 Lebofsky, L.A., Feierberg, M.A., Tokunaga, A.T., Larson, H.P. and Johnson, J.R., 1981. The 1.7-

566 to 4.2-micron spectrum of asteroid 1 Ceres: evidence for structural water in clay minerals.

567 Icarus. 48, 453–459.

568 Melchiorri, R., Encrenaz, T., Fouchet, T., Drossart, P., Lellouch, E., Gondet, B., Bibring, J.-P.,

569 Langevin, Y., Schmitt, B., Titov, D. and Ignatiev, N., 2007. Water vapor mapping on

570 Mars using OMEGA/Mars Express. Planet. Space Sci. 55. 333-342.

571 Michalski, J. R. and Niles, P. B., 2010. Deep crustal carbonate rocks exposed by meteoritic

572 impact on Mars. Nat. Geosci. 3, 751-755.

26

573 Milliken, R.E. and Rivkin, A.S., 2009. Brucite and carbonate assemblage from altered olivine-

574   rich materials on Ceres. Nat. Geosci. 2, 258-261.

575 Mittlefehldt, D.W., 1994. ALH84001, a cumulate othopyroxenite member of the Martian

576   meteorite clan. Meteoritics 29, 214–221.

577 Montes-H, G. and Geraud, Y. 2004. Sorption kinetic of water vapour of MX80 bentonite

578   submitted to different physical–chemical and mechanical conditions. Colloid Surface A.

579   235, 17-23.

580 Montes-H, G. and Rihs, S. 2006. A simplified method to estimate kinetic and thermodynamic

581   parameters on the solid–liquid separation of pollutants. J. Colloid Interf. Sci. 299, 49-55.

582 Montes-Hernandez, G., Fernandez-Martinez, A. and Renard, F. 2009. Novel Method to Estimate

583   the Linear Growth Rate of Submicrometric Calcite Produced in a Triphasic Gas-Liquid-

584   Solid System. Cryst. Growth Des. 9, 4567-4573.

585 Montes-Hernandez, G., Pommerol, A., Renard, F., Beck, P., Quirico, E. and Brissaud, O., 2010a.

586   In situ kinetic measurements of gas-solid carbonation of $Ca(OH)_2$ by using infrared

587   microscope coupled to a reaction cell. Chem. Eng. J. 161, 250-56.

588 Montes-Hernandez, G., Daval, D., Chiriac, R. and Renard, F., 2010b. Growth of Nanosied

589   Calcite through Gas-Solid Carbonation of Nanosized Portlandite under Anisobaric

590   Conditions. Cryst. Growth Des. 10, 4823-4830.

591 Montes-Hernandez, G., Chiriac, R., Toche, F. and Renard, F., 2012a. Gas–solid carbonation of

592   Ca(OH)2 and CaO particles under non-isothermal and isothermal conditions by using a

27

593   thermogravimetric analyzer: Implications for CO2 capture . Int. J. Greenh. Gas. Con. 11,

594   4172-180.

595   Montes-Hernandez, G., Daval, D., Findling, N., Chiriac, R. and Renard, F., 2012b. Linear growth

596   rate of nanosized calcite synthesized via gas–solid carbonation ofCa(OH)2 particles in a

597   static bed reactor. Chem. Eng. J. 180, 237-244

598   Morris, R.V., Ruff, S.W., Gellert, R., Ming, D.W., Arvidson, R. E.,Clark, B.C., Golden, D. C.,

599   Siebach, K., Klingelhöfer, G., Schröder, C., Fleischer, I., Yen, A.S. and Squyres, S.W.,

600   2010. Identification of Carbonate-Rich Outcrops on Mars by the Spirit Rover. Science

601   .329, 421-424.

602   Murchie, S.L., Mustard, J.F. Ehlmann, B.L., Milliken, R.E., Bishop, J.L., McKeown, N.K., Noe

603   Dobrea, E.Z., Seelos, F.P., Buczkowski, D.L., Wiseman, S.M., Arvidson, R.E., Wray, J.J.,

604   Swayze, G., Clark, R.N., Des Marais, D.J., McEwen, A.S. and Bibring, J.-P., 2009. A

605   synthesis of Martian aqueous mineralogy after 1 Mars year of observations from the Mars

606   Reconnaissance Orbiter. J.Geophys. Res.114, E00D06.

607   Mustard, J.F., Murchie, S.L., Pelkey, S.M., Ehlmann, B.L., Milliken, R.E., Grant, J.A., Birbing,

608   J.-P., Poulet, F., Bishop, J., Noe Dobrea, E., Seelos, F., Arvidson, R.E., Wiseman, S.,

609   Green, R., Humm, D., Malaret, E., McGovern, J.A., Seelos, K., Clancy, T., Clark, R., Des

610   Marais, D., Izenberg, N., Knudson, A., Langevin, Y., Martin, T., McGuire, P., Robinson,

611   M., Roush, T., Smith, M., Taylor, H., Titus, T. and Wolff, M., 2008. Hydrated silicate

612   minerals on Mars observed by the Mars Reconnaissance Orbiter CRISM instrument.

613   Nature. 454, 305-309

614   Ochs, D., Braun, B., Maus-Friedrichs, W. and Kempter, V. 1998a. CO2 chemisorption at Ca and

615   CaO surfaces: A study with MIES, UPS(HeI) and XPS. Surf. Sci .417,406–414.

616   Ochs, D., Brause, M., Braun, B., Maus-Friedrichs, W. and Kempter V.,1998b. CO2 chemisorp

617   tion at Mg and MgO surfaces: A study with MIES and UPS (He I). Surf .Sci., 397,101–

618   107.

619   Paquette, J. and Reeder, R.J., 1995. Relationship between surface structure, growth mechanism

620   and trace element incorporation in calcite. Geochem.Cosmochem. Acta. 59, 735-749.

621   Pommerol, A., Schmitt, B., Beck, P. and Brissaud, O., 2009. Water sorption on martian regolith

622   analogs: Thermodynamics and near-infrared reflectance spectroscopy. Icarus. 204, 114-

623   136.

624   Poulet, F., Bibring, J.-P., Langevin, Y., Mustard, J.F., Mangold, N., Vincendon, M., Gondet, B.,

625   Pinet, P., Bardintzeff, J.-M. And Platevoet, B., 2009. Quantitative compositional analysis

626   of martian mafic regions using the Mex/OMEGA reflectance data 1.Methodology,

627   uncertainties and examples of application. Icarus. 201, 69-83.

628   Rivkin, A.S., Volquardsen, E.L. and Clark, B.E., 2006. The surface composition of Ceres:

629   discovery of carbonates and iron-rich clays. Icarus. 185, 563–567

630   Rivkin, A.S., Li, J.Y., Milliken, R.E., Lim, L.F., Lovell, A.J., Schmidt, B.E., McFadden, L.A.

631   And Cohen, B.A., 2011. The surface composition of Ceres. Space Sci. Rev. 163, 95-116

632   Sala, M. , Delmonte, B., Frezzotti, M., Proposito, M., Scarchilli, C., Maggi, V., Artioli, G.,

633   Dapiaggi, M., Marino, F., Ricci, P.C. and De Giudici, G., 2008. Evidence of calcium

634   carbonates in coastal (Talos Dome and Ross Sea area) East Antarctica snow and firn:

635   Environmental and climatic implications. Earth Planet. Sci. Lett. 271, 43-52.

29

636 Santos, A., Ajbary, M., Morales-Flórez, V., Kherbeche, A., Pi˜nero, M. and Esquivias, L., 2009.

637   Larnite powders and larnite/silica aerogel composites as effective agents for CO2

638   sequestration by carbonation. J. Hazard. Mater. 168, 1397–1403.

639 Schorghofer, N. and Aharonson, O., 2005. Stability and exchange of subsurface ice on Mars. J.

640   Geophys. Res. 110, E05003.

641 Shaheen, R., Abramian, A., Horn, J., Dominguez, G., Sullivan, R. and Thiemens, M. H., 2010.

642   Detection of oxygen isotopic anomaly in terrestrial atmospheric carbonates and its

643   implications to Mars. Proceedings of the National Academy of Sciences of the United

644   States of America 107, 20213-20218.

645 Sigg, L., Xue, H., Kistker, D. and Schönenberger, R., 2000. Size fractionation (dissolved,

646   colloidal and particulate) of trace metals in the Thur River, Switzerland. Aquat. Geochem.

647   6, 413-434

648 Smith, M.D., 2002. The annual cycle of water vapor on Mars as observed by the Thermal

649   Emission Spectrometer. J. Geophys. Res. 107, E11,5115.

650 Smith, M.D., 2004. Interannual variability in TES atmospheric observations of Mars during

651   1999-2003. Icarus. 167, 148-165.

652 Smith, M.D., Wolff, M.J., Clancy, R.T. and Murchie, S.L., 2009. Compact Reconnaissance

653   Imaging Spectrometer observations of water vapor and carbon monoxide. J. Geophys.

654   Res. 114, E00D03.

655 Smith, P.H., Tamppari, L.K., Arvidson, R.E., Bass, D., Blaney, D., Boynton, W.V., Carswell, A.,

656   Catling, D.C., Clark, B.C., Duck, T., DeJong, E., Fisher, D., Goetz, W., Gunnlaugsson,

657   H.P., Hecht, M.H., Hipkin, V., Hoffman, J., Hviid, S.F., Keller, H.U., Kounaves, S.P.,

30

658   Lange, C.F., Lemmon, M.T., Madsen, M.B., Markiewicz, W.J., Marshall, J., McKay,

659   C.P., Mellon, M.T., Ming, D.W., Morris, R.V., Pike, W.T., Renno, N., Staufer, U.,

660   Stoker, C., Taylor, P., Whiteway, J.A. and Zent, A.P., 2009. H_2O at the Phoenix Landing

661   Site. Science .325, 58-61.

662 Stumm, W. and Morgan, J.J., 1995. , Aquatic Chemistry – Chemical Equilibria and Rates in

663 Natural Waters, John Wiley & Sons Inc., Third Edition, New York.

664 Thomas, P.C., Parker, J.Wm., McFadden, L.A., Russel, C.T., Stern, S.A., Sykes, M.V. and

665   Young, E.F., 2005. Differentiation of the asteroid Ceres as revealed by its shape. Nature.

666   437, 224-226.

667 Treiman, A. H., Amundsen, H. E. F., Blake, D. F. and Bunch, T., 2002. Hydrothermal origin for

668   carbonate globules in Martian meteorite ALH84001: a terrestrial analogue from

669   Spitsbergen (Norway). Earth Planet. Sci. Lett. 204, 323-332.

670 Vernazza, P., Mothé-Diniz, T., Barucci, M.A., Birlan, M., Carvano, J.M., Strazzulla, G.,

671   Fulchignoni, M. and Migliorini, A., 2005. Analysis of near-IR spectra of 1 Ceres and 4

672   Vesta, targets of the Dawn mission. Astron. Astrophys. 436, 1113–1121.

673 Xiong, Y. and Snider Lord, A., 2008. Experimental investigations of the reaction path in the

674    $MgO-CO_2-H_2O$ system in solutions with various ionic strengths, and their applications to

675   nuclear waste isolation. App. Geochem. 23, 1634–1659.

676 Yamamoto, S., Bluhm, H., Andersson, K., Ketteler, G., Ogasawara, H., Salmeron, M. and

677   Nilsson, A., 2008. In situ X-ray photoelectron spectroscopy studies of water on

678   metals and oxides at ambient conditions. J. Phys. Condens. Matt., 20, 184025-

679   184014.

31

680   Zolensky, M.E., Nakamura, K., Gounelle, M., Mikouchi, T., Kasama, T., Tachikawa, O. and

681   Tonui, E., 2002. Mineralogy of Tagish Lake : An ungrouped type 2 carbononaceous

682   chondrite. Meteorit. Planet. Sci. 37, 737-761.

683

684

685

686

687

688

689

690

691

692

693

694

695

696

697

698

699

700

701

702

703 Table 1. Summary of the experiments with their experimental conditions and the corresponding

704 kinetic parameters determined for gas-solid carbonation.

Exp.	Starting material	Gas pressure	temperature	$A^{CO3}_{,max1}$ (a.u.)	$A^{CO3}_{,max2}$ (a,u,)	$t_{1/2_1}$ (minutes)	$t_{1/2_2}$ (minutes)	Ea (kJ/mol)
1	portlandite	2 bar CO_2	-10°C	1.8	4.6	19.6	599.6	
2	portlandite	2 bar CO_2	0°C	6.4	0.8	8.9	8.9	43
3	portlandite	2 bar CO_2	10°C	5.3	11.4	61.8	61.8	
4	portlandite	2 bar CO_2	25°C	29.3	54.8	2.5	126.6	
5	portlandite	1 bar CO_2 + air	-10°C	2.5	5	3.7	33622	
6	portlandite	1 bar CO_2 + air	0°C	5.4	10.2	6.3	28.5	75
7	portlandite	1 bar CO_2 + air	10°C	15.8	3.1	3.5	180.1	
8	portlandite	1 bar CO_2 + air	30°C	26	21.2	3.5	5.8	
9	portlandite	100 mbar CO_2	25°C	19.8	10.9	0.8	419.1	
10	brucite	1 bar CO_2 + air	25°C	9.5	4.8	3	184.1	
11	Amorphous Ca silicate hydrate	1 bar CO_2 + air	25°C	8.9	68	<0.5	13.6	

Ea was calculated with Arrhenius equation. For experiments with 2 bar CO_2 ,we exclude the point of

10°C due to his incoherence with Arrhenius equation.

705

706

707

708

33

709

710

711

712

713
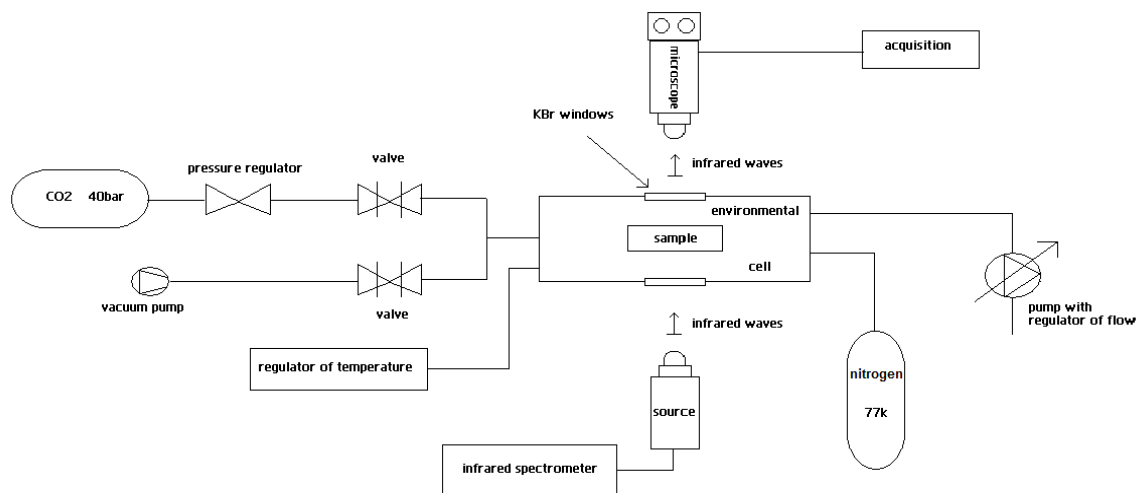
Figure 1 . Schematic representation of the IR-CryoCell experimental setup, showing the main parts such as temperature regulator, environmental cell, infrared microscope, valves, vacuum pump, CO_2 cylinder, liquid N_2 reservoir.

717

718

719
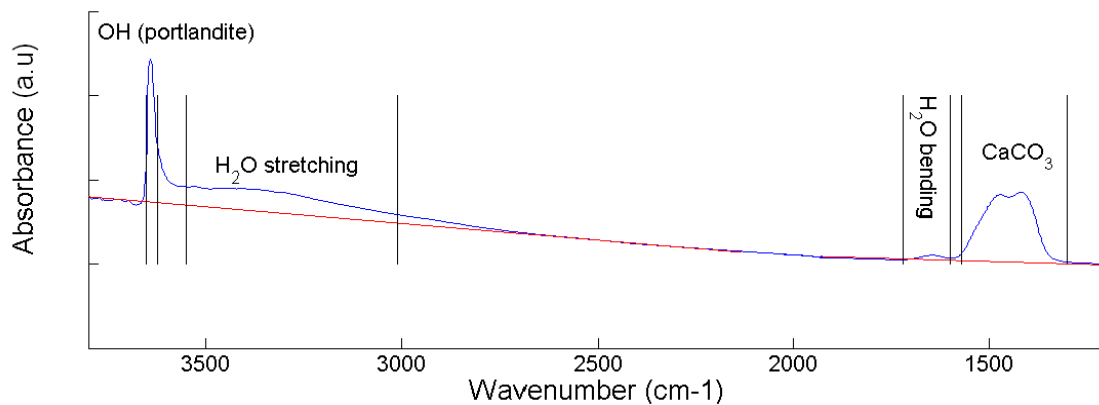
Figure 2 . Schematic representation for the calculation of the integrated band intensities of each functional group (-OH, H_2O, MCO_3), showing the continuum (in red) on an IR spectrum of portlandite.

738
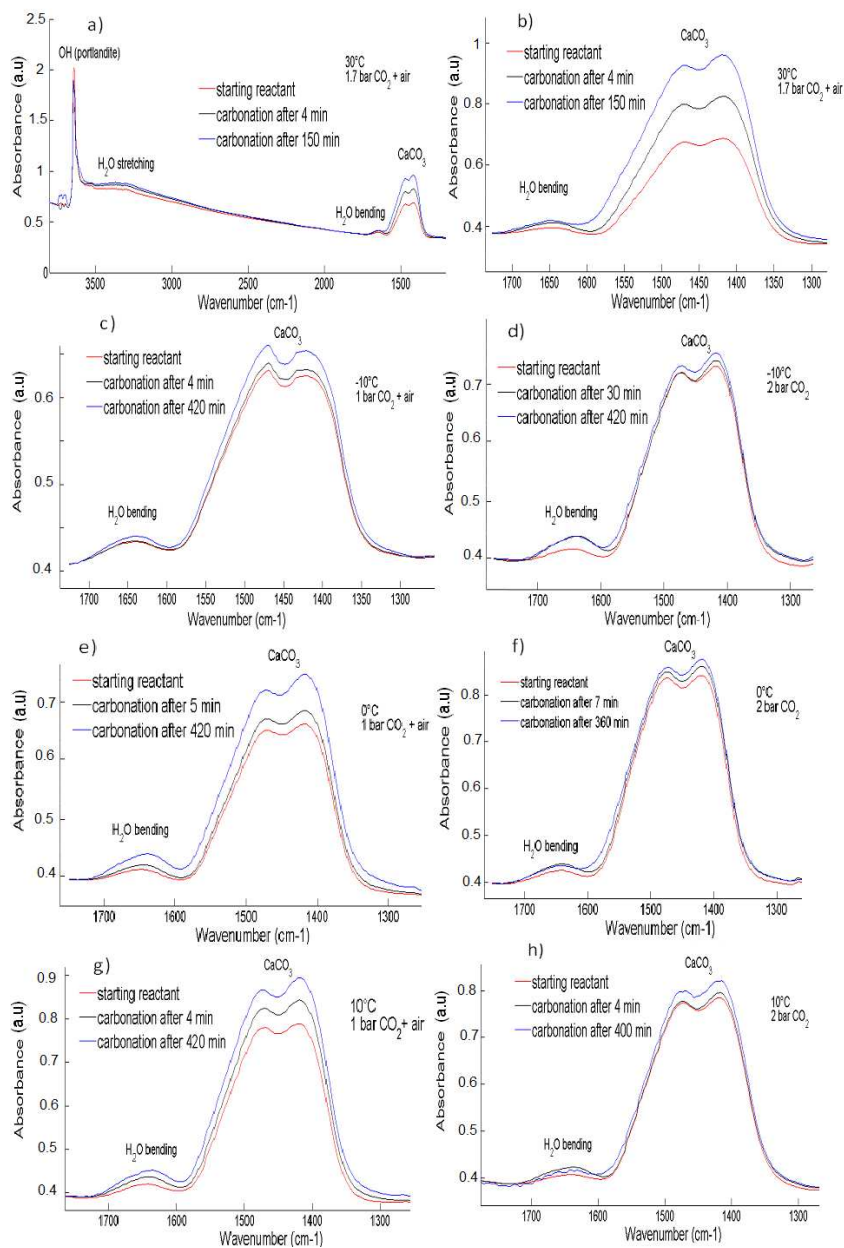
Figure 3. Evolution with time of the IR spectrum of calcium carbonate during carbonation at different temperatures and CO_2 pressures. a) Full IR spectrum of portlandite at 30°C with 1.7 bar of CO_2 in presence of air; (b) Carbonate band at 30°C under 1,7 bar of CO_2 with air; (c) at -10°C under 1bar of CO_2 with air ; (d) at -10°C under 2 bars of CO_2; (e) at 0°C under 1bar of CO_2 with air ; (f) at 0°C under 2bars of CO_2; (g) at 10°C under 1bar of CO_2 with air; (h) at 10°C under 2bars of CO_2.
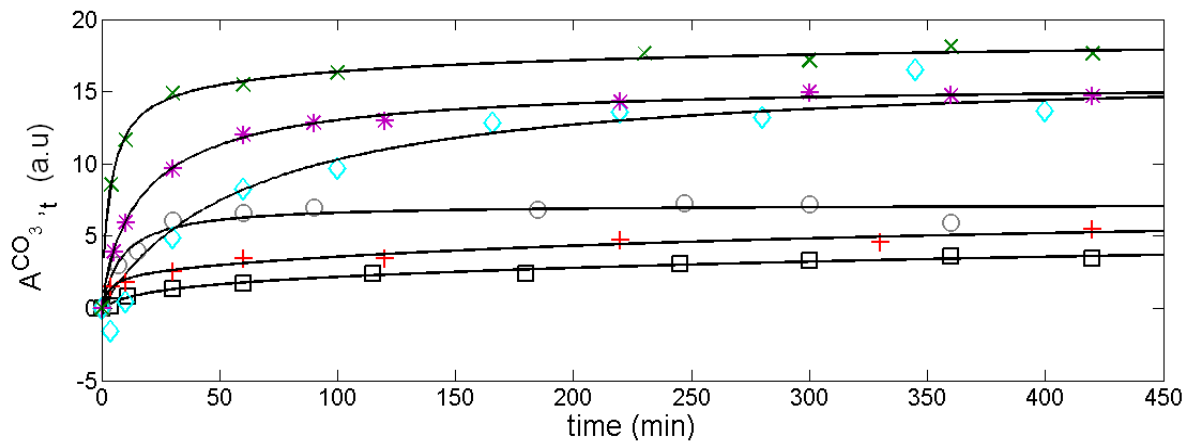
Figure 4. Fits of the experimental kinetic data (carbonate band intensity) for gas-solid carbonation of Ca hydroxide (portlandite) in various experimental conditions by using a kinetic double-pseudo-second-order model and applying the non-linear least squares method.
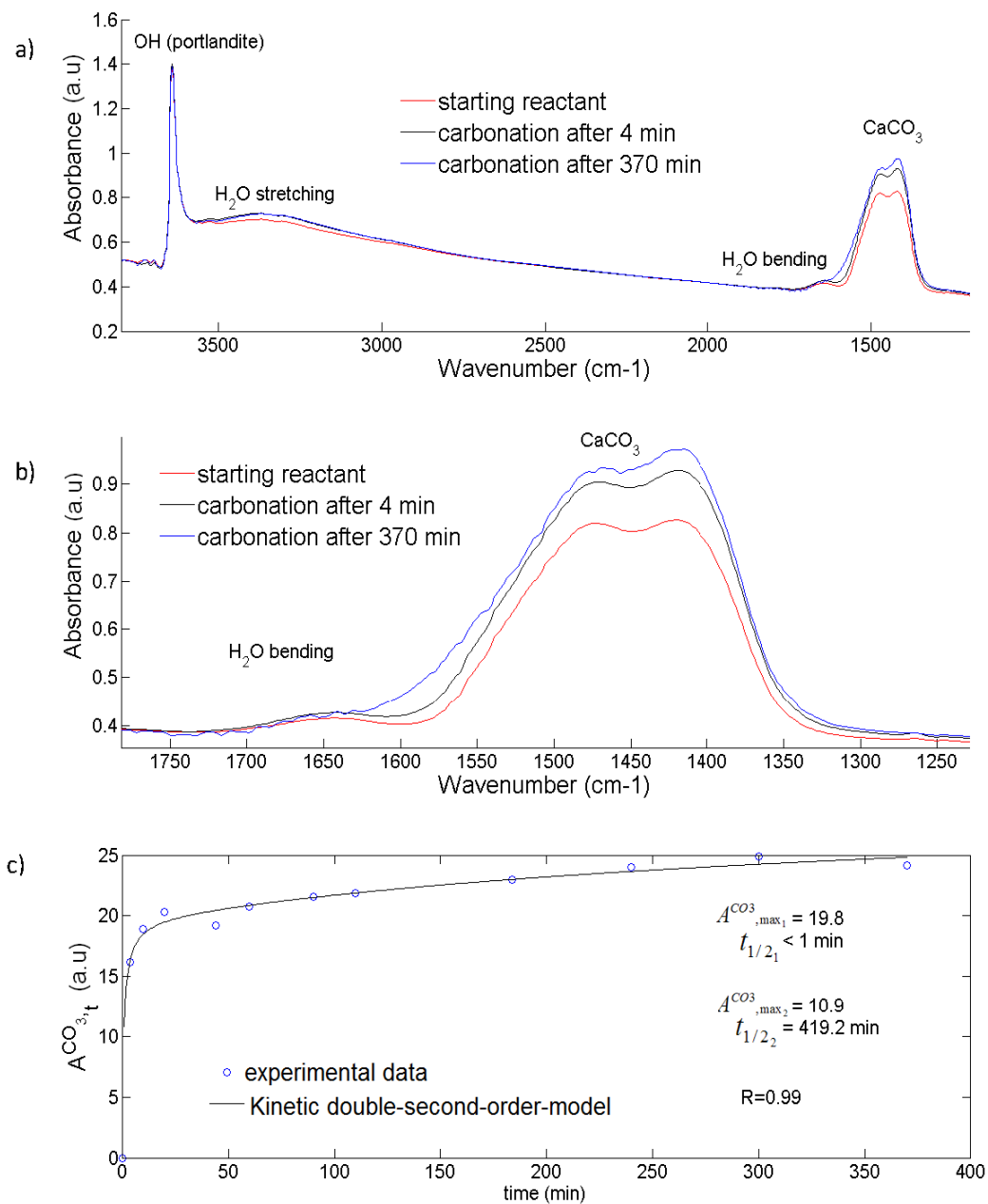
Figure 5. Evolution with time of the IR spectrum of Ca hydroxide (portlandite) during carbonation at 25°C under 100mbar of CO_2: a) Full spectrum. b) Band of the carbonate group. c) Fit of the experimental kinetic data (carbonate band intensity) for gas-solid carbonation by using a kinetic double-pseudo-second-order model and applying the non-linear least squares method.
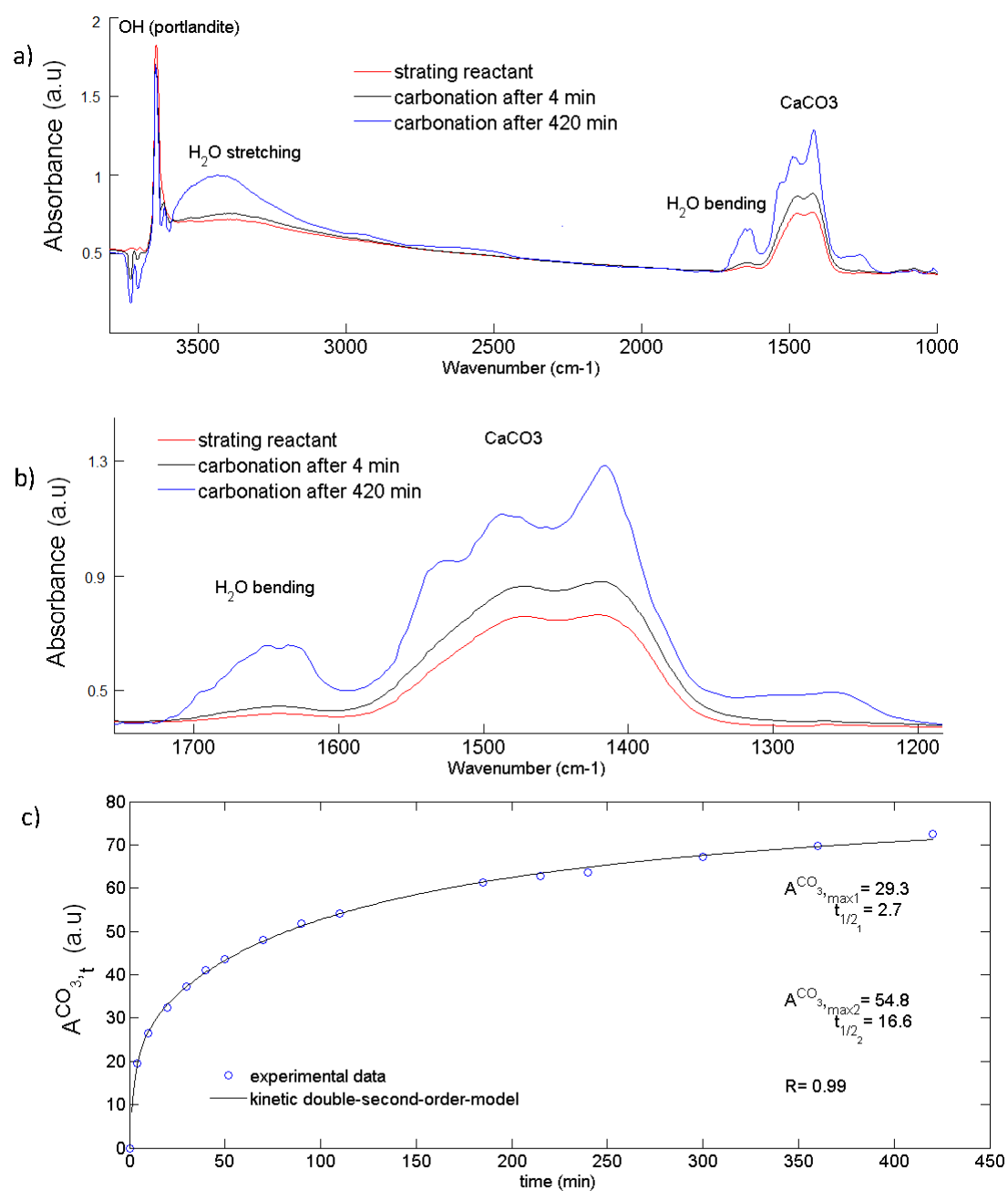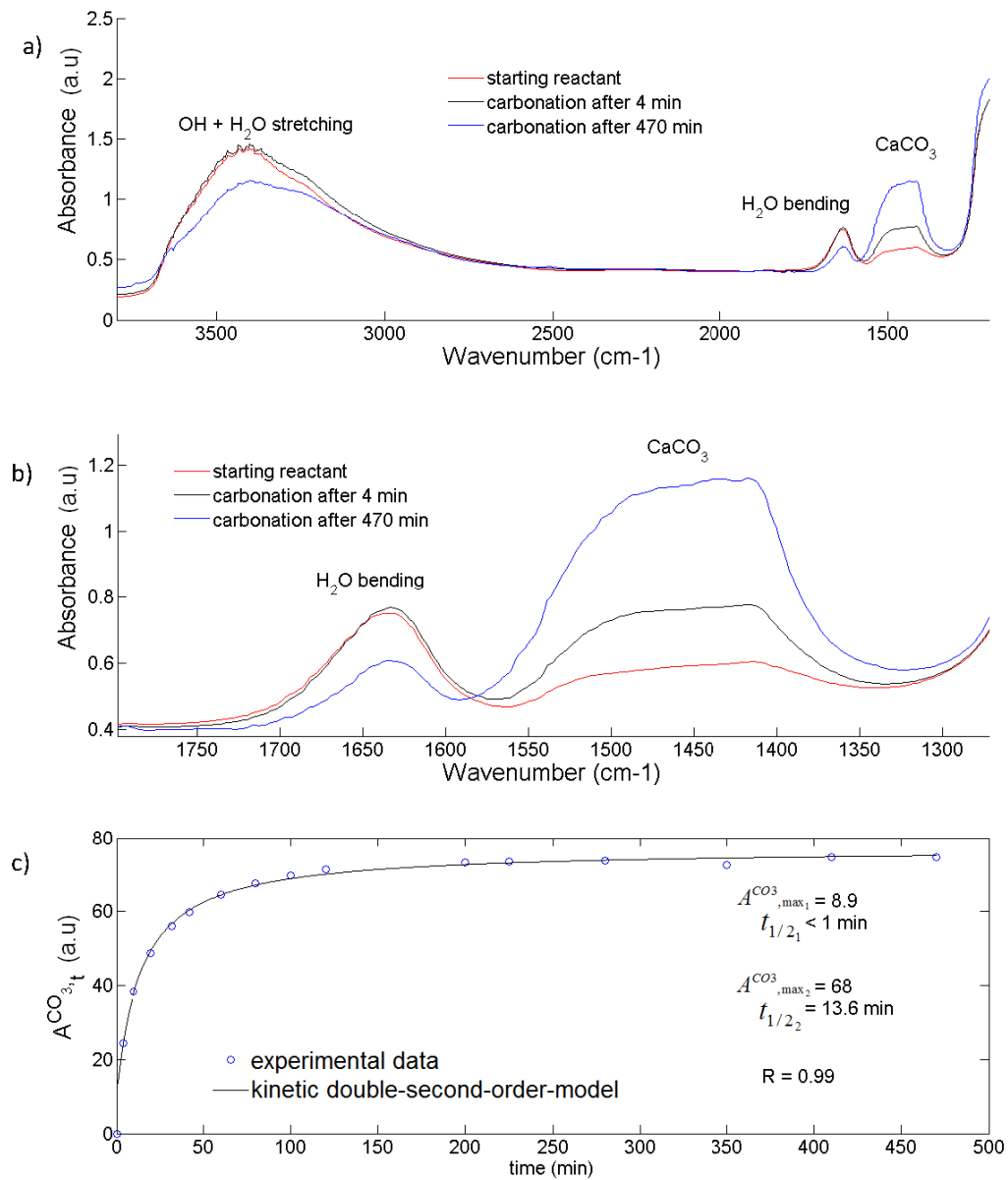
Figure 6. Evolution with time of the IR spectrum of Ca hydroxide (portlandite) during carbonation at 25°C under 2 bar of CO_2: a) Full spectrum. b) Band of the carbonate group. c) Fit of the experimental kinetic data (carbonate band intensity) for gas-solid carbonation by using a kinetic double-pseudo-second-order model and applying the non-linear least squares method.
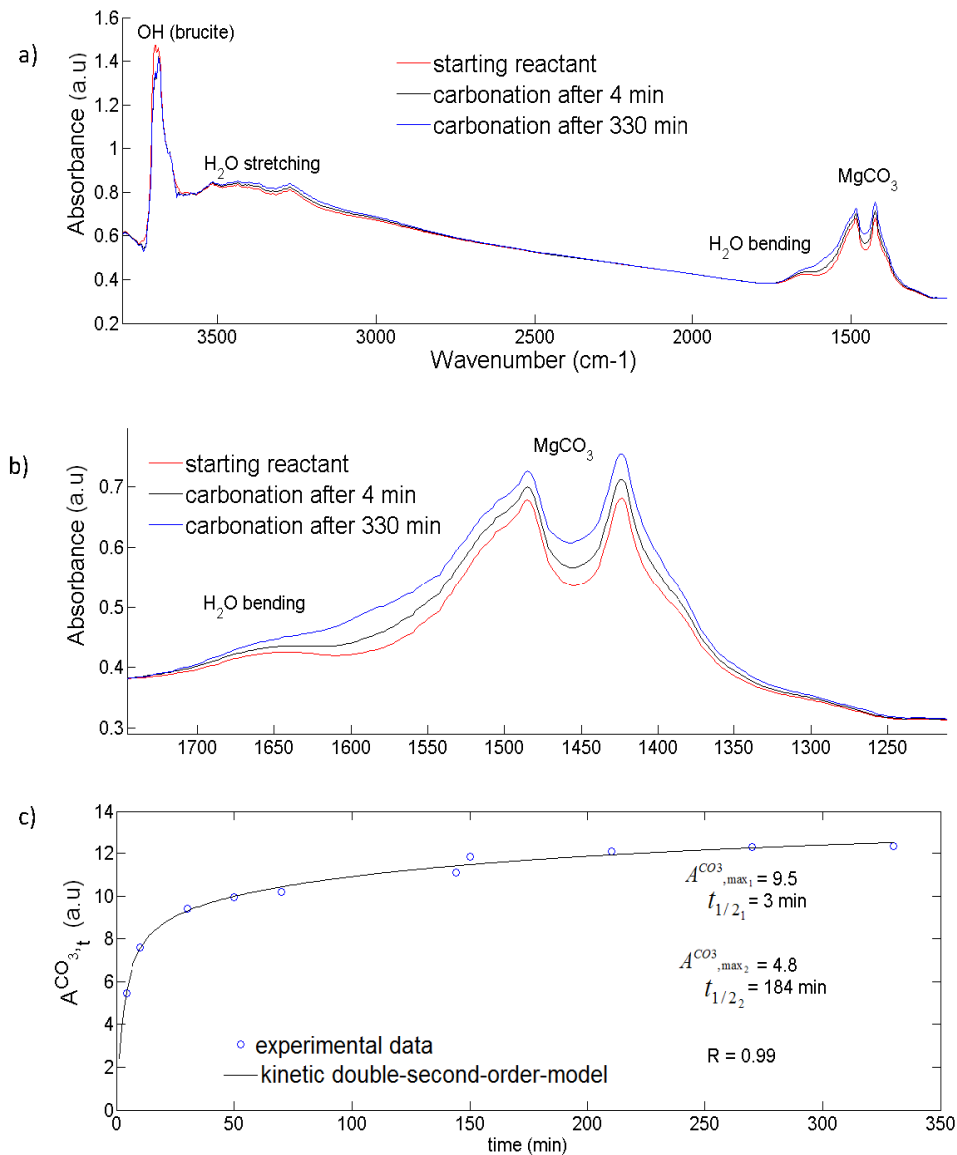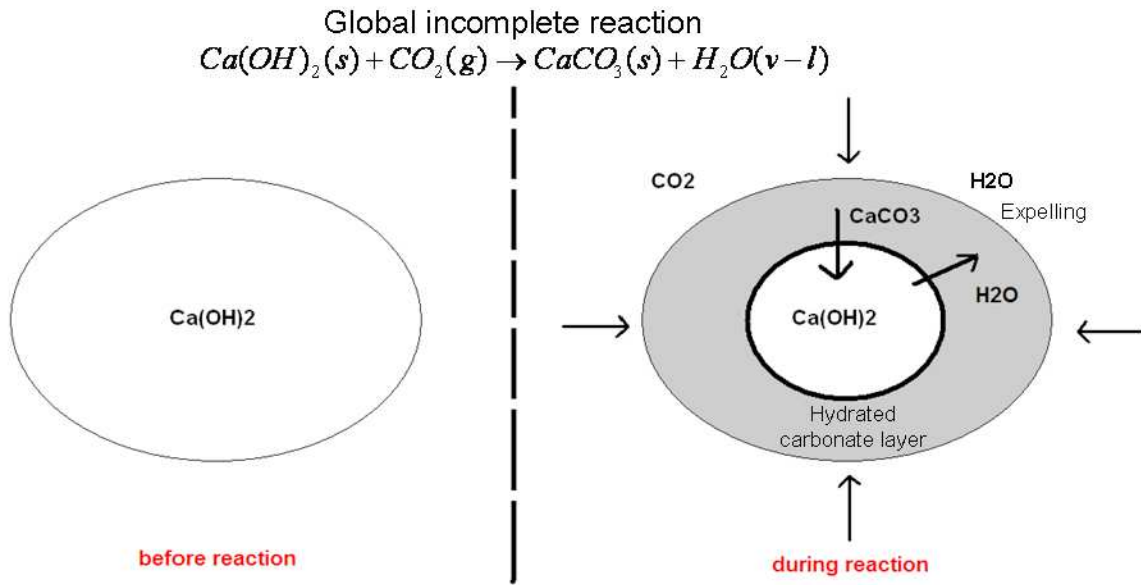
Figure 7. Evolution with time of the IR spectrum of the Mg hydroxide (brucite) during carbonation at 25°C under 1bar of CO_2 with air: a) Full spectrum. b) Band of the carbonate group c) Fit of the experimental kinetic data (carbonate band intensity) for gas-solid carbonation by using a kinetic double-pseudo-second-order model and applying the non-linear least squares method.

766

Figure 8. Evolution with time of the IR spectrum of amorphous Ca silicate hydrate during carbonation at 25°C under 1bar of CO_2 with air: a) Full spectrum. b) Band of carbonate group. c) Fit of the experimental kinetic data (carbonate band intensity) for gas-solid carbonation by using a kinetic double-pseudo-second-order model and applying the non-linear least squares method.

767
768
769
770

771

772

773

774

Global incomplete reaction
$$Ca(OH)_2(s) + CO_2(g) \rightarrow CaCO_3(s) + H_2O(v-l)$$
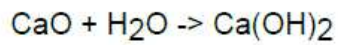
before reaction

during reaction

775

Figure 9. Schematic representation of the gas-solid carbonation of Ca hydroxide, showing the growth of a hydrated calcium carbonate layer and the expelling of molecular water.
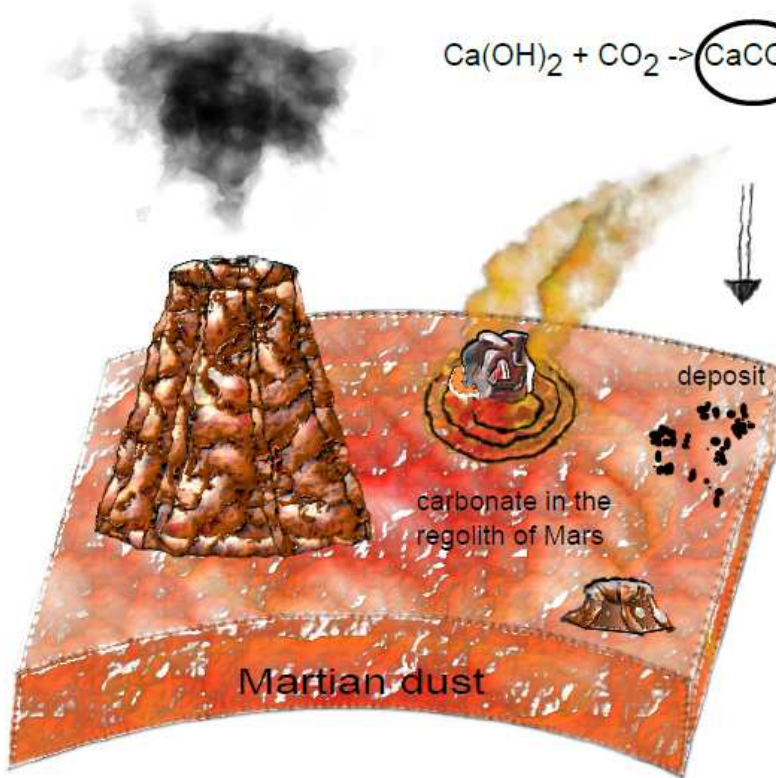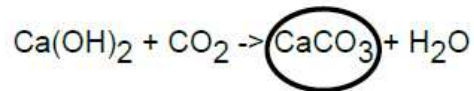
Binary oxides or amorphous silicates

atmospheric conditions are enough to
start the carbonation process

spontaneous hydration of precursor

$$CaO + H_2O \rightarrow Ca(OH)_2$$

unstable and react with atmospheric CO_2

$$Ca(OH)_2 + CO_2 \rightarrow \boxed{CaCO_3} + H_2O$$

deposit

carbonate in the
regolith of Mars

Martian dust

Figure 10. A schematic representation of a possible current formation mechanism at dust-CO2 interfaces of the calcium carbonate found at the Martian surface.

43